LETTER

doi:10.1038/nature11660

An early and enduring advanced technology originating 71,000 years ago in South Africa

Kyle S. Brown[1,2], Curtis W. Marean[2], Zenobia Jacobs[3], Benjamin J. Schoville[2], Simen Oestmo[2], Erich C. Fisher[2], Jocelyn Bernatchez[2], Panagiotis Karkanas[4] & Thalassa Matthews[5]

There is consensus that the modern human lineage appeared in Africa before 100,000 years ago[1,2]. But there is debate as to when cultural and cognitive characteristics typical of modern humans first appeared, and the role that these had in the expansion of modern humans out of Africa[3]. Scientists rely on symbolically specific proxies, such as artistic expression, to document the origins of complex cognition. Advanced technologies with elaborate chains of production are also proxies, as these often demand high-fidelity transmission and thus language. Some argue that advanced technologies in Africa appear and disappear and thus do not indicate complex cognition exclusive to early modern humans in Africa[3,4]. The origins of composite tools and advanced projectile weapons figure prominently in modern human evolution research, and the latter have been argued to have been in the exclusive possession of modern humans[5,6]. Here we describe a previously unrecognized advanced stone tool technology from Pinnacle Point Site 5–6 on the south coast of South Africa, originating approximately 71,000 years ago. This technology is dominated by the production of small bladelets (microliths) primarily from heat-treated stone. There is agreement that microlithic technology was used to create composite tool components as part of advanced projectile weapons[7,8]. Microliths were common worldwide by the mid-Holocene epoch, but have a patchy pattern of first appearance that is rarely earlier than 40,000 years ago[9,10], and were thought to appear briefly between 65,000 and 60,000 years ago in South Africa and then disappear. Our research extends this record to ~71,000 years, shows that microlithic technology originated early in South Africa, evolved over a vast time span (~11,000 years), and was typically coupled to complex heat treatment that persisted for nearly 100,000 years. Advanced technologies in Africa were early and enduring; a small sample of excavated sites in Africa is the best explanation for any perceived 'flickering' pattern.

Microlithic technology varies worldwide and is often defined regionally[9]. Microlithic is used to describe small stone blades (bladelets) retouched to create highly standardized shapes (backed blades or segments), or assemblages with high frequencies of small tools[10]. We follow Clark's concise technological definition: the process of manufacture (core reduction) is focused on the production of small flakes and bladelets less than 50 mm in maximum length[7] (Supplementary Discussion). Microlithic technology has been considered more typical of the Later Stone Age (LSA) and Upper Palaeolithic phase postdating 45 kyr in Africa and Eurasia, respectively, atypical for the Middle Stone Age (MSA) in Africa (300–45 kyr), absent in the Middle Palaeolithic in Eurasia, and potentially a universal stage in the evolution of Palaeolithic technologies[10].

Backed blade technology occurs earliest in Africa. The oldest East African sites with microliths are the Naisiusiu Beds at Olduvai Gorge, Enkapune Ya Muto, and Mumba rockshelter. The Naisiusiu Beds have infinite radiocarbon ages of >45 kyr[11] and electron spin resonance (ESR) ages of 59 ± 5 kyr and 62 ± 5 kyr[12]. The earliest Enkapune Ya Muto (Endingi) microlithic has a calibrated radiocarbon age of ≥45 kyr[8]. The oldest backed blades at Mumba rockshelter (Tanzania) are dated by optically stimulated luminescence (OSL) to 57 ± 5 kyr[13]. Small numbers of backed blades come from Twin Rivers in Zambia[14], but the age is contested[15,16]. The Howiesons Poort (HP) in southern Africa is well represented by many samples, meets the Clark definition of microlithic technology (Fig. 1), and is well constrained by large numbers of OSL ages to between 60 and 65 kyr[17].

The microlithic technology we report is from Pinnacle Point Site 5–6 (PP5–6) on the south coast of South Africa (Supplementary Fig. 1 and Supplementary Discussion). The deposits we report here come

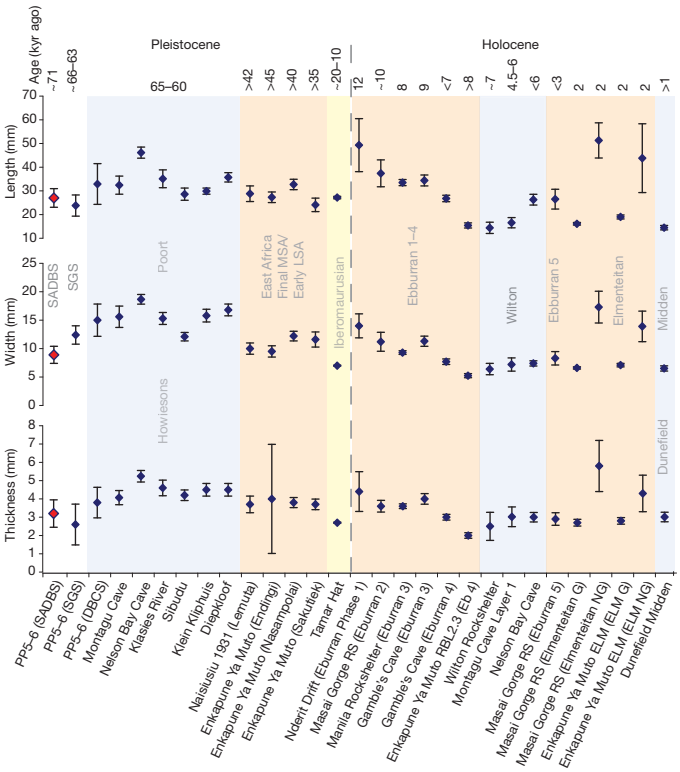

Figure 1 | Segment dimensions from PP5–6 and selected late Pleistocene and Holocene sites. Mean and error bars showing 95% confidence intervals for segment dimensions were calculated for segment length, width and thickness using published sample mean ($\bar{x}$), standard deviation (s) and sample count (n) values from selected African assemblages. The equation for calculating the 95% confidence interval is: $\bar{x} \pm t_{0.05}(n-1) * s/\sqrt{n}$, in which $t_{0.05}$ is the value at probability 0.05 at $(n-1)$ degrees of freedom from a two-tailed t-table. The values for $t_{0.05}$ were calculated using the TINV function in Microsoft Excel. Sources for data described are in Supplementary Information.

[1]Department of Archaeology, University of Cape Town, Rondebosch 7701, South Africa. [2]Institute of Human Origins, School of Human Evolution and Social Change, PO Box 872402, Arizona State University, Tempe, Arizona 85287-4101, USA. [3]Centre for Archaeological Science, School of Earth and Environmental Sciences, University of Wollongong, Wollongong 2522, Australia. [4]Ephoreia of Palaeoanthropology-Speleology of Southern Greece, Arditou 34b, 11636 Athens, Greece. [5]Department of Natural History, Iziko South African Museum, PO Box 61, Cape Town 8000, South Africa.

from the Long Section at PP5–6 (ref. 18), a ~14 m (vertical) continuous sediment stack revealed by nine ~two-month seasons of excavation. Combined with 76 OSL samples and total station piece-plotting, the PP5–6 Long Section provides a high resolution sequence to investigate the age and character of technological change. A brief overview of the major strata and ages surrounding and containing the microlithic strata follows (see Supplementary Discussion). The Shelly Ashy Dark Brown Sand (SADBS) contains the oldest microlithic assemblage (Fig. 2). The SADBS is underlain by the aeolian Ashy Light Brown Sand (ALBS) with a weighted mean OSL age of 71.1 ± 2.3 kyr ($n = 6$). The SADBS has a weighted mean age of 70.6 ± 2.3 kyr ($n = 6$). The top of the SADBS is an eroded surface overlain by the Orange Brown Sand 1 (OBS1) with a weighted mean OSL age of 66.0 ± 2.8 kyr ($n = 3$). The Shelly Gray Sand (SGS) overlies the OBS1 and is beneath the Dark Brown Compact Sand (DBCS) with three OSL ages ranging from 58 ± 4 to 65 ± 4 kyr. The Reddish Brown Sand and Roofspall (RBSR) caps the sequence with seven statistically consistent OSL ages, and a weighted mean age of 53.9 ± 1.7 kyr. Most microliths reported here were plotted directly by total station with millimetre accuracy, whereas the others come from small lenses also constrained by total station measurements. Outstanding contextual control is provided through total station plotting combined with field stratigraphy, three-dimensional geographic information system (GIS) analysis of plotted finds, and soil and sediment micromorphology (Supplementary Discussion).

The HP is present at PP5–6 in the DBCS with a range of backed and notched tool forms (Supplementary Fig. 2), heat-treated silcrete (80%)[18], and an age consistent with other HP occurrences[17]. Core reduction focused on the production of small blades (mean length 27 mm); some retouched into backed blade segments (symmetric tools that are backed (blunted) on one side and sharp on the other (Fig. 3)) and notched pieces (Supplementary Table 1). DBCS segments (silcrete = 8, chert = 3) have dimensions (mean length 33 mm) similar to those of other HP sites in southern Africa (Fig. 1). Notched pieces are a common retouched tool form in the HP sample from Klasies River[19,20], are common in the DBCS, and are rare in the underlying SADBS. The DBCS has single and double platform silcrete cores that were reduced to a relatively small size (mean length 30 mm). The SGS stratum has a small but dense sample of lithics with backed pieces (Supplementary Fig. 3) and three irregular notched pieces. The small sample of SGS segments ($n = 5$) has the shortest mean length (24 mm) in comparison to those of the DBCS and SADBS (Fig. 1). There are few diagnostic tools in the OBS1, probably owing to the fragmented assemblage and abundance of quartz. There are two small crescents at the base of the OBS1, similar in form to those of the SADBS (Supplementary Figs 3 and 4).

The SADBS lithic assemblage is dominated by small blade products that are significantly shorter ($t(167) = 2.06$, $P = 0.02$) and narrower ($t(167) = 2.23$, $P = 0.01$) than those of the DBCS (one-tailed Student's t-test). SADBS blade length and width are also statistically different from the Klasies River HP when compared across 95% confidence intervals of the means (Supplementary Fig. 5 and Supplementary Table 2). SADBS blades have plain platforms typically with abrasion on the platform edge adjacent to the flaking surface, and are made almost exclusively on silcrete and other non-quartzite raw materials. Crested blades and small unidirectional and bidirectional blade cores support the characterization of the SADBS as a bladelet-focused assemblage. SADBS formal tools are segments made from small silcrete and chert blades (Supplementary Fig. 4), with mean length/width ratios significantly higher than those of the DBCS (HP) (Mann–Whitney $U = 17$, exact $P = 0.006$). SADBS, SGS and DBCS segments have coefficient of variation values for length that are in the range of segment values for other HP and LSA Wilton (Holocene) tool assemblages (Supplementary Table 3).

We conducted a comparative analysis of segments between the PP5–6 samples, HP assemblages and more recent archaeological sites throughout Africa. SADBS segment dimensions (Supplementary Table 4) are within the 95% confidence intervals for segments at the MSA and LSA boundary in East Africa, the Tamar Hat Iberomaurusian in North Africa

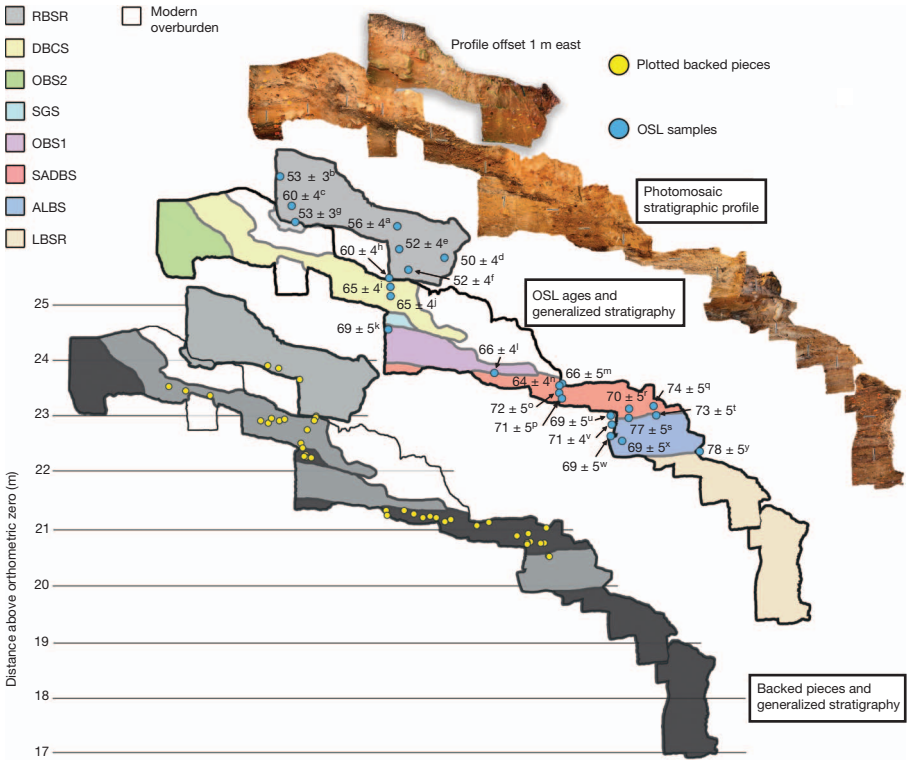

Figure 2 | PP5–6 stratigraphic aggregates. Photomosaic of the upper 8 m of stratigraphy (top), total station plotted OSL sample locations (middle) and locations and association of total station plotted microlithic segments (bottom). Age superscript corresponds to superscript with sample codes presented in Supplementary Table 5. The excavated archaeological deposit extends below what is depicted in the figure.

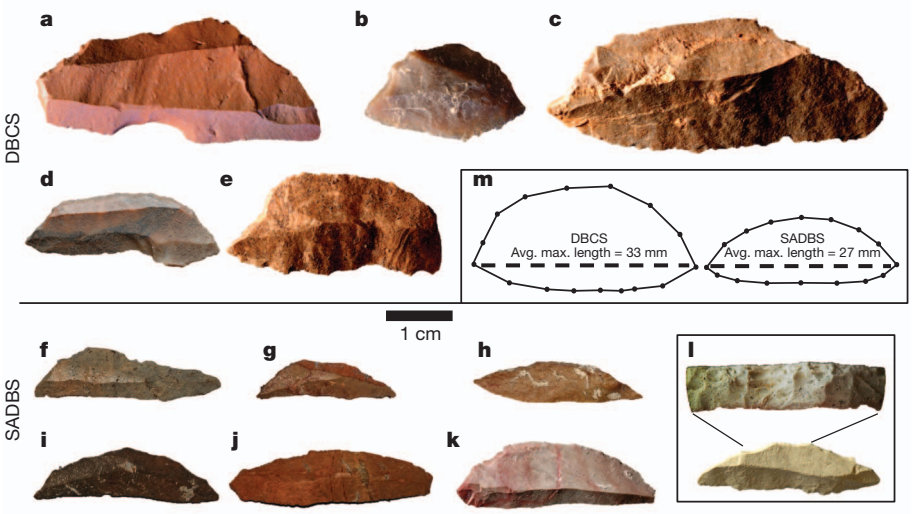

Figure 3 | PP5–6 microlithic tools. **a**–**l**, Representative images of PP5–6 segments from the DBCS (HP; **a**–**e**) and SADBS (**f**–**k**), showing differences in size and shape, and fine flaking of the backed edge (**l**) on a segment from the OBS1. Backed blades are oriented with the backed edge up and the unmodified edge down. **m**, The average shape for each stratigraphic aggregate is shown scaled to the average maximum (avg. max.) length (DBCS on the left, SADBS on the right). The artefact plotted find numbers (project specimen numbers) are 121094 (**a**), 133878 (**b**), 266888 (**c**), 280295 (**d**), 266287 (**e**), 107536 (**f**), 259888 (**g**), 312237 (**h**), 151511 (**i**), 272915 (**j**), 155127 (**k**) and 177975 (**l**).

(~20–10 kyr), and Holocene assemblages in South and East Africa (Fig. 1). More easily flaked obsidian (owing to its lack of crystalline structure) dominates the East African assemblages, so despite a tougher raw material (silcrete) the SADBS knappers produced comparable microliths. SADBS segments are shorter and thinner than HP segments with no overlap in confidence intervals for width; they are more similar to East African LSA assemblages than the HP (Fig. 1). A shape analysis was performed using landmark-based geometric morphometrics (Supplementary Fig. 6), which focuses on complete form more effectively than conventional linear dimension analyses[21,22]. Shape analysis was performed on a more limited sample of sites because it required direct access to the artefacts or large samples of published segment images. The mean segment shape from the HP at PP5–6 is not significantly different from the Klasies River HP ($P = 0.07$, non-parametric testing, multivariate analysis of variance (MANOVA)). However, SADBS segment shape is significantly different from both PP5–6 HP ($P = 0.035$) and Klasies River HP ($P = 0.026$) (Supplementary Figs 7 and 8). At PP5–6 the SADBS is stratified below and substantially predates the HP, and, despite being older, is even more convergent on later classic microlithic forms than the HP.

The silcrete that dominates the SADBS and HP at PP5–6 was heat treated[18], a technique that is known to date back to ~162 kyr at Pinnacle Point 13B. The technological recipe for microlith production at PP5–6 follows this long complex chain: (1) collection of silcrete at patchily distributed sources; (2) collection and transport of appropriate wood fuel to heat treatment locations; (3) controlled temperature heat treatment of silcrete; (4) preparation of microblade cores on silcrete; (5) controlled production of bladelets; (6) reshaping of bladelets into microliths; (7) production of mounts on wood or bone; and (8) adhesion of microliths to form compound tools. The HP has been considered 'complex'[23] or 'exceptional'[24] and the disappearance of the HP advanced technology has been argued to reflect a transient pattern of technological complexity in Africa that flickers in and out of existence as a function of demography[3,4]. The thick high resolution sequence dated by large numbers of OSL ages at PP5–6 allows us to demonstrate technological continuity in the microlith production on heat-treated silcrete from ~71–60 kyr, showing retention of a recipe that requires high fidelity intergenerational transmission across a large region, whereas heat treatment technology persisted for nearly 100,000 years or more[18]. Backed blade, microlithic and heat treatment technologies may strengthen and weaken as preferred strategies, but the temporal span is vast, indicating that the cognitive capacity for culturally embedding and transmitting these complex recipes manifests early and persistently in southern Africa. The perceived transient pattern of advanced technologies probably reflects the very small sample of well-excavated sites in Africa, a sample that is a tiny fraction of the available European Middle Palaeolithic sample, and the need to study materials recovered from the smallest sieve fractions. Each new excavated site in Africa seems to chip away at this flickering pattern of advanced technologies.

SADBS microlithic backed bladelets differ in form from the previously described HP and are similar in linear dimensions to Holocene microlithic segments. The SADBS microliths document a commitment to microlithic technology 6,000 years before the HP, while also showing that the preferred bladelet form changed over time. On the basis of ethnographic analogy, these Holocene microliths were proposed to have tipped arrows[25,26]. However, microliths could also have been used to tip atlatl (spearthrower) darts[5,27]. Early modern humans in South Africa had the cognition to design and transmit at high fidelity these complex recipe technologies. This ability facilitated effective weapons grounded in microlithic technology, conferring increased killing distance and power over hand-cast spears[28]. Microlith-tipped projectile weapons increased hunting success rate, reduced injury from hunting encounters gone wrong, extended the effective range of lethal interpersonal violence[29], and would have conferred substantive advantages on modern humans as they left Africa and encountered Neanderthals equipped with only hand-cast spears[30].

METHODS SUMMARY

PP5–6 has been excavated from 2006–2012 creating a ~14 m vertical excavated section. To summarize briefly, the site is excavated in 50-cm quadrants, named by their bearing: NE, NW, SE and SW, within 1-m squares. Excavations follow natural stratigraphic units (for example, layers and features), and thus square–quadrant–stratigraphic unit provenience designation is the minimum assigned to any find. All observed finds were plotted directly to total station in three dimensions, and the rest were captured by nested 10–3–1 mm wet-sieving.

OSL dating determines burial ages for sediments based on the increase in the number of trapped electrons in mineral grains with increasing time after burial, in response to the energy supplied by background levels of ionizing radiation from environmental sources. The time elapsed since sediments were last exposed to sufficient heat or sunlight to empty the relevant electron traps can be estimated from measurements of the OSL signal, together with determinations of the radioactivity of the sample and the material surrounding it to a distance of ~50 cm. The

burial dose ('equivalent dose', D_e) can be measured using the OSL signal from a sample of sediment and represents the radiation dose to which sedimentary grains have been exposed in their burial environment. The dose rate (D_r) represents the rate of exposure of these grains to ionizing radiation over the entire period of burial; this dose is mostly derived from the radioactive decay of ^{238}U, ^{235}U, ^{232}Th (and their daughter products) and ^{40}K, with lesser contributions from cosmic rays and from radioactive inclusions internal to the dated mineral grains. The burial age of grains that were well bleached by sunlight at the time of deposition can then be calculated from the D_e divided by the D_r.

Full Methods and any associated references are available in the online version of the paper.

Received 22 August; accepted 5 October 2012.
Published online 7 November 2012.

1. Blum, M. G. B. & Jakobsson, M. Deep divergences of human gene trees and models of human origins. *Mol. Biol. Evol.* **28,** 889–898 (2011).
2. Endicott, P., Hob, S. Y. W. & Stringer, C. Using genetic evidence to evaluate four palaeoanthropological hypotheses for the timing of Neanderthal and modern human origins. *J. Hum. Evol.* **59,** 87–95 (2010).
3. d'Errico, F. & Stringer, C. Evolution, revolution or saltation scenario for the emergence of modern cultures? *Phil. Trans. R. Soc. B* **366,** 1060–1069 (2011).
4. Powell, A., Shennan, S. & Thomas, M. Late Pleistocene demography and the appearance of modern human behavior. *Science* **324,** 1298–1301 (2009).
5. Sisk, M. L. & Shea, J. J. The African origin of complex projectile technology: an analysis using tip cross-sectional area and perimeter. *Int. J. Evol. Biol.* **2011,** 968012 (2011).
6. Brooks, A. S., Nevell, L., Yellen, J. E. & Hartman, G. in *Transitions Before the Transition* (eds Hovers, E. & Kuhn, S. L.) 233–255 (Springer, 2006).
7. Clark, J. D. in *Recent Advances in Indo-Pacific Prehistory* (eds Misra, V. N. & Bellwood, P.) 95–101 (E. J. Brill, 1985).
8. Ambrose, S. Small things remembered: origins of early microlithic industries in Sub-Saharan Africa. *Archaeol. Papers Am. Anthropol. Assoc.* **12,** 9–29 (2002).
9. Kuhn, S. & Elston, R. Introduction: thinking small globally. *Archaeol. Papers Am. Anthropol. Assoc.* **12,** 1–7 (2002).
10. Kuhn, S. Pioneers of microlithization: the "proto-Aurignacian" of Southern Europe. *Archaeol. Papers Am. Anthropol. Assoc.* **12,** 83–94 (2002).
11. Manega, P. C. *Geochronology, Geochemistry and Isotopic Study of the Plio-Pleistocene Hominid Sites and the Ngorongoro Volcanic Highland in Northern Tanzania*. PhD thesis, Univ. Colorado (1993).
12. Skinner, A. R., Hay, R. L., Masao, F. & Blackwell, B. A. B. Dating the Naisiusiu Beds, Olduvai Gorge, by electron spin resonance. *Quat. Sci. Rev.* **22,** 1361–1366 (2003).
13. Gliganic, L. A., Jacobs, Z., Roberts, R. G., Domínguez-Rodrigo, M. & Mabulla, A. Z. P. New ages for Middle and Later Stone Age deposits at Mumba rockshelter, Tanzania: optically stimulated luminescence dating of quartz and feldspar grains. *J. Hum. Evol.* **62,** 533–547 (2012).
14. Barham, L. Backed tools in Middle Pleistocene central Africa and their evolutionary significance. *J. Hum. Evol.* **43,** 585–603 (2002).
15. Herries, A. I. R. A chronological perspective on the Acheulian and its transition to the Middle Stone Age in Southern Africa: the question of the Fauresmith. *Int. J. Evol. Biol.* **2011,** 1–25 (2011).
16. Barham, L. Clarifying some fundamental errors in Herries' "a chronological perspective on the Acheulian and its transition to the Middle Stone Age in southern Africa: the question of the Fauresmith. *Int. J. Evol. Biol.* **2012,** 1–5 (2012).
17. Jacobs, Z. *et al.* Ages for the Middle Stone Age of Southern Africa: implications for human behavior and dispersal. *Science* **322,** 733–735 (2008).
18. Brown, K. S. *et al.* Fire as an engineering tool of early modern humans in coastal South Africa. *Science* **325,** 859–862 (2009).
19. Singer, R. & Wymer, J. *The Middle Stone Age at Klasies River Mouth in South Africa* (Univ. of Chicago Press, Chicago, 1982).
20. Wurz, S. The Howiesons Poort backed artefacts from Klasies River: an argument for symbolic behavior. *S. Afr. Archaeol. Bul.* **54,** 38–50 (1999).
21. Adams, D. C. *et al.* Geometric morphometrics: ten years of progress following the 'revolution'. *Ital. J. Zool. (Modena)* **71,** 5–16 (2004).
22. Rohlf, F. J. tpsDig Version 2.10. http://life.bio.sunysb.edu/morph/index.html (2006).
23. Mellars, P. Major issues in the emergence of modern humans. *Curr. Anthropol.* **30,** 349–385 (1989).
24. Bar-Yosef, O. & Kuhn, S. The big deal about blades: laminar technologies and human evolution. *Am. Anthropol.* **101,** 322–338 (1999).
25. Clark, J. D., Phillips, J. & Staley, P. S. Interpretations of prehistoric technology from ancient Egyptian and other sources. Part I: ancient Egyptian bows and arrows and their relevance for African prehistory. *Paleorient* **2,** 323–388 (1974).
26. Clark, J. D. Interpretations of prehistoric technology from ancient Egyptian and other sources. Part II: prehistoric arrow forms in Africa as shown by surviving examples of traditional arrows of the San Bushmen. *Paleorient* **3,** 127–150 (1975).
27. Pétillon, J.-M. *et al.* Hard core and cutting edge: experimental manufacture and use of Magdalenian composite projectile tips. *J. Archaeol. Sci.* **38,** 1266–1283 (2011).
28. Shea, J. The origins of lithic projectile point technology: evidence from Africa, the Levant, and Europe. *J. Archaeol. Sci.* **33,** 823–846 (2006).
29. Bingham, P. M. Human evolution and human history: A complete theory. *Evol. Anthropol.* **9,** 248–257 (2000).
30. Churchill, S. E., Franciscus, R., McKean-Peraza, H., Daniel, J. & Warren, B. Shanidar 3 Neandertal rib puncture wound and paleolithic weaponry. *J. Hum. Evol.* **57,** 163–178 (2009).

Supplementary Information is available in the online version of the paper.

Acknowledgements We thank the MAPCRM staff for their assistance, the Dias Museum for field facilities, and SAHRA and HWC for permits. This research was funded by the National Science Foundation (grants BCS-9912465, BCS-0130713, BCS-0524087 and BCS-1138073 to C.W.M.), the Hyde Family Foundation, the Institute of Human Origins (IHO), and the Australian Research Council (DP1092843 to Z.J.).

Author Contributions K.S.B. led the lithic analysis and with C.W.M. took the lead in writing the paper; J.B. contributed to the site analysis; E.C.F. conducted the GIS analysis and photomosaic construction; C.W.M. is the project director and an excavation permit co-holder; S.O. contributed to the lithic analysis; B.J.S. contributed to the lithic analysis and conducted the morphometric analysis; Z.J. conducted the OSL dating; P.K. studied the sedimentology and geology of the site; T.M. is an excavation permit co-holder and contributes to palaeoenvironmental studies; and J.B., K.S.B., E.C.F., C.W.M., S.O. and B.J.S. all contributed substantially to the excavations. All authors contributed to the writing of the paper.

Author Information The data reported in this paper are tabulated in the Supplementary Information and archived at Arizona State University. Reprints and permissions information is available at www.nature.com/reprints. The authors declare no competing financial interests. Readers are welcome to comment on the online version of the paper. Correspondence and requests for materials should be addressed to C.W.M. (curtis.marean@asu.edu.).

METHODS

Excavation methods. PP5–6 has been excavated from 2006–2011 as part of the South African Coast Paleoclimate, Paleoenvironment, Paleoecology, Paleoanthropology Project (SACP4), creating a ~14 m vertical excavated section. All excavations are conducted using published protocols[31–34]. To summarize briefly, the site is excavated in 50-cm quadrants within squares, named by their bearing: NE, NW, SE and SW. Excavations follow natural stratigraphic units (for example, layers and features), and thus square–quadrant–stratigraphic unit provenience designation is the minimum assigned to any find. Sediment volumes were measured during excavation, and bulk samples of sediment were taken from every unique stratigraphic unit. All observed finds were plotted directly to total station in three dimensions, and the rest were captured by nested 10–3–1 mm wet-sieving. Laboratory processing of materials from PP5–6 is still in progress and thus most analyses involving archaeological specimens are limited to piece-plotted artefacts that have been catalogued and analysed up to the date of submission.

OSL dating methods. OSL dating determines burial ages for sediments[35–40]. The method is based on the increase in number of trapped electrons in mineral grains (such as quartz) with increasing time after burial, in response to the energy supplied by background levels of ionizing radiation from environmental sources. The time elapsed since sediments were last exposed to sufficient heat or sunlight to empty the relevant electron traps can be estimated from measurements of the OSL signal, together with determinations of the radioactivity of the sample and the material surrounding it to a distance of ~50 cm. The burial dose ('equivalent dose', D_e) can be measured using the OSL signal from a sample of sediment, which can be as small as a single sand-sized grain, and represents the radiation dose to which sedimentary grains have been exposed in their burial environment. The dose rate (D_r) represents the rate of exposure of these grains to ionizing radiation over the entire period of burial; this dose is mostly derived from the radioactive decay of ^{238}U, ^{235}U, ^{232}Th (and their daughter products) and ^{40}K, with lesser contributions from cosmic rays and from radioactive inclusions internal to the dated mineral grains. The burial age of grains that were well bleached by sunlight at the time of deposition can then be calculated from D_e divided the D_r.

Shape analysis methods. Dorsal view artefact images were digitized with two landmarks at technologically homologous points where the backed edge intersects the unretouched edge on the proximal and distal ends (Supplementary Fig. 6). Seven sliding semi-landmarks were then placed along both the backed and sharp edges to capture the shape of curves between landmarks[41]. Procrustes superimposition analysis was performed and displayed using the thin-plate spline programs available from Rohlf[22]. This removes differences in size, orientation and image positioning. A relative warps, or principal components, analysis on the shape variables provides an indication of the relationship in shape space of the SADBS segments with those of the DBCS. The average shape is the origin point, and the deformation grids at each axis end illustrate the direction of shape change along those vectors (Supplementary Fig. 7). PC1 along the x axis separates narrower SADBS tools from rounded crescent shaped HP tools.

Stratigraphic photomosaic method. The PP5–6 Long Section photomosaic (Fig. 2) compiles 486 photographs taken in nine-image high definition range (HDR) sets spanning −4 to +4 exposure value (EV) captured with a Nikon D300S camera with flashes arranged to limit shadows and stabilize the lighting conditions. The photos were shot at f11, maintaining a focal distance of 25 cm, and providing an image resolution <0.5 cm. Photo rectification chits placed onto the profile at ~20 cm spacing provided systematic tie points between the overlapping images. We used the Adobe Lens Calibration Utility to develop a personalized geometric lens distortion and vignetting correction. Corrections were made in Adobe Lightroom 3 and the corrected NEF images were exported as TIFFs. We used Enfuse GUI v2.1 for HDR processing.

Photographic areas not part of the stratigraphic section were digitally masked from each 0EV image using Adobe Photoshop CS5. Removal of these areas was necessary to minimize parallactic stitching distortion and did not alter the appearance or morphology of the stratigraphy visible within the images. The masks applied to the 0EV images were then applied to each equivalent HDR image. The masked 0EV images were mosaicked using PTGUI v9.0.4 to interpolate patterns between each image. ECF subsequently refined the image matching using photo chits and other prominent landmarks across images. The geometrically warped image stack was exported to Photoshop and mosaicked using the 'auto-blend' function to create seamless layer masks that were then individually refined and checked. The processing steps were repeated on the HDR images using the 0EV file as a template to provide an exact copy of the geometric warp and mosaic. The 0EV final layer masks were applied to the HDR image layers, thereby creating two identical photomosaic profiles, 0EV and HDR. Linear colour and sharpening enhancements of the final profile were as follows: a high-pass filter (radius = 10 pixels) was applied to the HDR mosaic and overlaid onto the 0EV mosaic image to provide linear sharpening and texture enhancement. Colour and contrast enhancement was accomplished by duplicating the final 0EV mosaic and overlaying it atop itself, adjusting the transparency of the overlay image to 50%.

The final mosaic was georectified in ESRI ArcGIS10 using the image photo rectification chits. The spline method was used to warp image mosaic to the 2D photo chit point locations with a root mean square < 0.01. The full photo mosaic was subdivided into six panels and converted to 2.5 dimensions by texture mapping each panel onto an equivalently-sized polygon in Google Sketchup. The true three-dimensional location of the lower right corner of each panel provided an anchor to project each Sketchup plate within the three-dimensional GIS in its proper spatial position.

31. Marean, C. W. *et al.* Paleoanthropological investigations of Middle Stone Age sites at Pinnacle Point, Mossel Bay (South Africa): Archaeology and hominid remains from the 2000 Field Season. *PaleoAnthropol.* **83,** 14–83 (2004).
32. Dibble, H. L. *et al.* The use of barcodes in excavation projects. *SAA Archaeol. Rec.* **7,** 33–38 (2005).
33. Marean, C. W. *et al.* The stratigraphy of the Middle Stone Age sediments at Pinnacle Point Cave 13B (Mossel Bay, Western Cape Province, South Africa). *J. Hum. Evol.* **59,** 234–255 (2010).
34. Bernatchez, J. & Marean, C. W. Total station archaeology and the use of digital photography. *SAA Archaeol. Rec.* **11,** 16–21 (2011).
35. Huntley, D. J., Godfrey-Smith, D. I. & Thewalt, M. L. W. Optical dating of sediments. *Nature* **313,** 105–107 (1985).
36. Aitken, M. J. *An Introduction to Optical Dating* (Oxford Univ. Press, 1998).
37. Duller, G. A. T. Luminescence dating of Quaternary sediment: recent developments. *J. Quat. Sci.* **19,** 183–192 (2004).
38. Lian, O. B. & Roberts, R. G. Dating the Quaternary: progress in luminescence dating of sediments. *Quat. Sci. Rev.* **25,** 2449–2468 (2006).
39. Jacobs, Z. & Roberts, R. G. Advances in optically stimulated luminescence dating of individual grains of quartz from archeological deposits. *Evol. Anthropol.* **16,** 210–223 (2007).
40. Wintle, A. G. Fifty years of luminescence dating. *Archaeometry* **50,** 276–312 (2008).
41. Bookstein, F. L. Landmark methods for forms without landmarks: morphometrics of group differences in outline shape. *Med. Image Anal.* **1,** 225–243 (1997).